Secondary Electron Spectra from Dielectric Theory

By DAVID K. BRICE *and* PETER SIGMUND

Det Kongelige Danske Videnskabernes Selskab
Matematisk-fysiske Meddelelser **40**:8

Kommissionær: Munksgaard
København 1980

This work was supported in part by
the Danish Natural Science Research Council
and the U.S. Department of Energy, DOE,
under Contract AT(29-1) 789.

Synopsis

Angular and energy distributions of electrons excited by a heavy charged particle penetrating an electron gas have been studied theoretically for a range of electron densities. The calculations are based on the self-consistent dielectric theory of Lindhard in which the properties of the electron gas are described by a frequency and wave-vector dependent dielectric function. The excitation cross section has been investigated in the present work for a broad range of incident projectile velocities, and numerical results are presented both for doubly and singly differential forms of the excitation spectrum. An analytical approximation is developed for the case of low projectile velocities, and comparison with numerical results indicates that the analytical form is quite adequate for velocities up to near the Fermi velocity. For higher incident velocities the emitted energy spectrum is characterized by a resonance for electron energies in the range ~ 1–4 times the Fermi energy; at electron energies about 10 times the Fermi energy the spectrum approaches that given by the Rutherford cross section. The electron energy at which the resonance occurs is independent of the projectile velocity, but is a slowly varying function of the electron density. The angular position of the resonance is, however, a strong function of the projectile velocity, occurring first in the forward direction at a critical velocity, v_c, moving to higher angles with increasing projectile velocity, and limiting to lateral (90°) emission at high incident velocity. These results may form a basis for more detailed studies of electron emission in both atom-atom and atom-solid collisions.

DAVID K. BRICE[1] PETER SIGMUND[2]
H. C. Ørsted Institute,
DK-2100 Copenhagen Ø., Denmark

1: Permanent address:
Sandia Laboratories
Albuquerque, New Mexico, 87185, USA

2: Present address:
Physics Institute,
Odense University
DK-5230 Odense M, Denmark

Printed in Denmark by Bianco Lunos Bogtrykkeri A-S. ISSN 0023-3323. ISBN 87-7304-106-8

Table of contents

1. Introduction

The free electron gas is a convenient system for model studies of atomic and solid-state properties. In particular, this system offers unique possibilities of studying the interaction of energetic charged particles with matter, as far as the interaction with electrons is concerned. The free electron gas in the self-consistent picture developed by Lindhard[1] allows a treatment of the stopping of a charged particle with essentially no limitations on the range of particle velocities to be considered, thus giving qualitative insight into the partition of energy that would be quite difficult to obtain by other means.[2] When combined with the Thomas-Fermi principle, this dielectric theory provides estimates of stopping parameters that exhibit basic scaling properties as a function of atomic number.[3,4]

The dielectric theory has implications on the excitation spectrum of an electron gas. While collective excitations (plasma modes) occur in rather well-defined energy quanta, and thus show up in a number of well-studied phenomena,[5] the situation is different with regard to single-particle excitations. In a free electron gas, single-particle excitations form a continuous spectrum. Therefore most discrete systems would seem to call for a more elaborate treatment, unless attention is given to high levels of excitation and, especially, ionization. These phenomena have received less attention from the point of view of the dielectric theory than the stopping process.

In the present study, the spectrum of electrons excited by an energetic charged particle has been analyzed within the framework of the dielectric theory. Both energy and angular distributions of electrons have been evaluated as a function of the velocity of the primary particle. Therefore, the information extracted from the model is more specific than the predictions on energy loss, where primary velocity and Fermi velocity are the only variables. Both the capabilities of, and limitations to the model are expected to show up more clearly in differential quantities than in integrated ones.

Our main motivation for this study was a need for universal, and not necessarily very accurate angular and energy distributions of electrons after excitation by charged particles. Such spectra are called for in the analysis of a wide range of phenomena in radiation physics, chemistry, and biology.[6] Although quantitative studies have been made of specific systems, both experimental and theoretical,

we were missing the qualitative guidelines that the dielectric model provides in stopping theory. We started with a numerical evaluation of doubly differential electron spectra from the dielectric theory, similar to what was done by Ritchie et al. [7,8] for the energy spectrum. Later the numerical evaluation of electron spectra was followed up by an analytical study. The theory in its present form, we believe, provides insight into the qualitative behavior of secondary-electron spectra from light-ion bombardment, in particular the possible occurrence of peaks in the energy and angular distributions, the correlation between the energy and angular distribution as a function of particle velocity, and the range of angles that is accessible for secondary electrons at any given set of particle and electron energies. We had hoped to present Thomas-Fermi scaled spectra at the same time, but with an increasing amount of available analytical results we found that within the time limits imposed, it seemed most appropriate to present the free-electron results separately, and reserve applications to a later occasion.

2. Basic Equations

The basic equation governing the excitation of secondary electrons by a charged particle traversing a degenerate Fermi-Dirac gas of electrons has been derived by Ritchie.[9] His primary attention was directed toward the effects of the target on the incident projectile, and consequently the secondary electron spectrum has not been discussed in great detail. In the present section we will present a brief derivation of the basic equations for both the excitation cross section and for the single-particle contribution to the stopping cross section. Our procedure differs from that of Ritchie, but is consistent with Lindhard's derivation of the dielectric function. The derivation also makes evident the limitations of the procedure, and serves to introduce the notation which will be used throughout the paper.

A. *The Model*

We consider a point particle of charge e_1 and velocity $\boldsymbol{v}$, which traverses a degenerate Fermi-Dirac gas of electrons. The fractional energy and momentum losses suffered by the particle through its interaction with the system are assumed to be small over a time period which is long compared with pertinent electronic periods, so that $\boldsymbol{v}$ can be taken as a constant. This assumption will be quite good for a massive particle traversing the system, or for a highly energetic particle with mass comparable with the electron mass. The charge density, $\varrho(\boldsymbol{r},t)$ asso-

ciated with the perturbing particle is given by

$$\varrho(\boldsymbol{r},t) = e_1 \delta(\boldsymbol{r} - \boldsymbol{v}t) . \tag{2.1}$$

where δ represents the Dirac delta function.

The local electric potential $\Phi(\boldsymbol{r},t)$ which results from the charge density (2.1) includes the Coulomb field of the incident projectile as well as the induced field which results from the dynamic response of the electronic system to the perturbation. In the self-consistent treatment of Lindhard[1] the many-body problem of the interaction between an incident projectile and the electrons and between the electrons of the system themselves is resolved in the dielectric function $\varepsilon(\boldsymbol{k},\omega)$ of the system. By definition, $\varepsilon(\boldsymbol{k},\omega)$ connects $\Phi(\boldsymbol{r},t)$ and $\varrho(\boldsymbol{r},t)$ through the relation

$$\Phi(\boldsymbol{k},\omega) = 4\pi\varrho(\boldsymbol{k},\omega)/k^2\varepsilon(\boldsymbol{k},\omega) , \tag{2.2}$$

where $\Phi(\boldsymbol{k},\omega)$ and $\varrho(\boldsymbol{k},\omega)$ are the Fourier transforms of $\Phi(\boldsymbol{r},t)$ and $\varrho(\boldsymbol{r},t)$, respectively. For a function $g(\boldsymbol{r},t)$, the Fourier transform $g(\boldsymbol{k},\omega)$ is defined such that

$$g(\boldsymbol{r},t) = (VT)^{-1} \sum_{\boldsymbol{k},\omega} g(\boldsymbol{k},\omega) e^{i(\boldsymbol{k}\cdot\boldsymbol{r}-\omega t)}, \tag{2.3}$$

where periodic boundary conditions in the volume V and time interval T are assumed. Both V and T are taken to be large, and will ultimately be allowed to limit to infinity.

Equations (2.1)–(2.3) give the perturbing potential

$$\Phi(\boldsymbol{r},t) = \frac{4\pi e_1}{V} \sum_{\boldsymbol{k},\omega} \frac{\delta_{\boldsymbol{k}\cdot\boldsymbol{v},\omega} e^{i(\boldsymbol{k}\cdot\boldsymbol{r}-\omega t)}}{k^2\varepsilon(\boldsymbol{k},\omega)} . \tag{2.4}$$

$\Phi(\boldsymbol{r},t)$ as given in Eqn. (2.4) is the effective interaction potential between the incident projectile and the electrons of the system. This field is the generalization for the system of electrons of the Coulomb interaction between two isolated charged particles.

B. *The Dielectric Function*

The dielectric function $\varepsilon(\boldsymbol{k},\omega)$ has been evaluated for the free Fermi gas by Lindhard[1] within first-order time-dependent perturbation theory. The electrons of the system are assumed to occupy states described by single-particle free-electron wave functions, $\psi(\boldsymbol{r},t)$, where

$$\psi(\boldsymbol{r},t) = V^{-1/2} e^{i(\boldsymbol{k}\cdot\boldsymbol{r}-\omega t)} . \tag{2.5}$$

The single-particle energies, E, are given by

$$E = \frac{\hbar^2 k^2}{2m} = \hbar\omega \tag{2.6}$$

where $\hbar$ is Planck's constant divided by 2π and m the electron mass. The system is taken initially to be in its ground state so that all states are occupied up to the Fermi energy ε_F given by

$$\varepsilon_F = \frac{1}{2} m v_F^2 = \frac{\hbar^2 k_F^2}{2m} = \frac{\hbar^2}{2m} (3\pi^2 n)^{2/3} \tag{2.7}$$

where n is the electron density in the system, and v_F and k_F are the magnitudes of the velocity and wave vector, respectively, of electrons having energy ε_F.

The results of Lindhard's analysis are conveniently expressed in terms of the variables u, z, and χ^2, defined by

$$u = \omega / k v_F \tag{2.8a}$$

$$z = k / 2k_F \tag{2.8b}$$

and

$$\chi^2 = e^2 / (\pi \hbar v_F) , \tag{2.9}$$

where e is the electronic charge. In these variables

$$\varepsilon(\boldsymbol{k}, \omega) = 1 + \frac{\chi^2}{z^2} [f_1(u,z) + i f_2(u,z)] \tag{2.10}$$

where

$$f_1(u,z) = \frac{1}{2} + \frac{1}{8z} \left\{ [1-(z+u)^2] \ln \left| \frac{z+u+1}{z+u-1} \right| \right.$$
$$\left. + [1-(z-u)^2] \ln \left| \frac{z-u+1}{z-u-1} \right| \right\}. \tag{2.11}$$

and

$$f_2(u,z) = \begin{cases} \dfrac{\pi u}{2} & \text{for} \quad |z+u| < 1 , \qquad (2.12a) \\ \dfrac{\pi}{8z} [1-(z-u)^2] & \text{for} \quad |z-u| < 1 < |z+u| \qquad (2.12b) \\ 0 & \text{otherwise.} \qquad (2.12c) \end{cases}$$

C. *The Transition Rates*

The excitation spectrum and the stopping cross section can be obtained from the perturbing potential, Eqn. (2.4), and electron wave functions, Eqn. (2.5), through a straightforward application of first-order time dependent perturbation theory. The use of first-order theory is valid as long as the transition rates remain small, and it is consistent with Lindhard's form of the dielectric function. It is our aim in the present work to discuss some qualitative features of the single-electron excitation spectrum, and therefore we disregard higher order effects[10], as well as many-body corrections to the Lindhard dielectric function.

In the present section we will write

$$E(\boldsymbol{k}) = E_0\,; \quad \boldsymbol{k} = \boldsymbol{k}_0\,; \quad \omega = \omega_0 = E_0/\hbar \tag{2.13a}$$

for the initial electronic states (i.e., for $|\boldsymbol{k}| < k_F$), and

$$E(\boldsymbol{k}) = E_1\,; \quad \boldsymbol{k} = \boldsymbol{k}_1\,; \quad \omega = \omega_1 = E_1/\hbar \tag{2.13b}$$

for the final states ($|\boldsymbol{k}| > k_F$). If $W(\boldsymbol{k}_1)d^3k_1$ represents the probability per unit time for excitation of electrons into states $\boldsymbol{k}_1$ in the $\boldsymbol{k}$-space volume element d^3k_1, then first-order time-dependent perturbation theory yields

$$W(\boldsymbol{k}_1)\,d^3k_1 = 2\frac{2\pi}{\hbar}N_1(E_1)\,dE_1\,d\Omega_1 \sum_{\boldsymbol{k}_0}\left|\frac{4\pi e_1 e}{Vk^2\varepsilon(\boldsymbol{k},\boldsymbol{k}\cdot\boldsymbol{v})}\right|^2 \cdot \delta(E_1 - E_0 - \hbar\boldsymbol{k}\cdot\boldsymbol{v})\,, \tag{2.14}$$

where $\boldsymbol{k} = \boldsymbol{k}_1 - \boldsymbol{k}_0$, $N_1(E_1)$ is the density of states at E_1, and $d\Omega_1$ a solid angle at $\boldsymbol{k}_1$. The extra factor of two in front of the standard expression comes from the sum over spin states which are not altered by the potential (2.4). For large V the sum in (2.14) can be expressed as an integral through

$$\sum_{\boldsymbol{k}} \rightarrow \frac{V}{(2\pi)^3}\int d^3k \tag{2.15a}$$

and, likewise

$$N_1(E_1)\,dE_1 = \frac{V}{(2\pi)^3}k_1^2 dk_1\,. \tag{2.15b}$$

This yields

$$W(\boldsymbol{k}_1)\,d^3k_1 = \frac{e_1^2 e^2}{\hbar^2\pi^3}d^3k_1\int d^3k_0\left|\frac{1}{k^2\varepsilon(\boldsymbol{k},\boldsymbol{k}\cdot\boldsymbol{v})}\right|^2\delta(\omega_1 - \omega_0 - \boldsymbol{k}\cdot\boldsymbol{v})\,. \tag{2.16}$$

The integration over vectors $\boldsymbol{k}_0$ is restricted to $k_0 < k_F$. The transition rate can also be expressed as a cross section $d^3\sigma(\boldsymbol{k}_1)$ by

$$d^3\sigma(\boldsymbol{k}_1) = \frac{W(\boldsymbol{k}_1)}{nv}\, d^3k_1. \tag{2.17}$$

Eqn. (2.16) has already been derived by Ritchie (Eqn. (4.14) in ref. 9; his equation contains a spurious factor $\hbar^{-1}$).

The introduction of a cross section according to eq. (2.17) should at this point be taken as a formal step that will allow a direct comparison with the corresponding single-electron (or binary-encounter) cross sections at all stages of the theory. The physical significance of a single-electron cross section in a theory that takes into account the mutual interaction between target electrons is less evident, and we do not claim that there is any in a strict sense. Both Lindhard[1,2] and Ritchie[7-9] and coworkers avoid introducing such cross sections altogether and restrict their analysis to quantities characterizing the interaction with the medium rather than with the individual electron. Thus, any cross sections discussed in the following become physically meaningful when multiplied by the electron density n to become inverse mean free paths.

D. *The Stopping Cross Section*

Lindhard and Winther[2] have previously discussed in detail the stopping cross section $S(v)$ of the free electron gas for an incident charged particle. They take as a starting point for their discussion the electric field resulting from the potential of Eqn. (2.4) which acts to retard the motion of the incident particle.[11,1] The contribution of the single-particle excitations to the stopping cross section can also be found from the above excitation cross section.

The basic transition probability is multiplied by the energy transfer $\hbar\omega$ *before* summation over the initial states. An extra factor of $\hbar\omega = \hbar\boldsymbol{k}\cdot\boldsymbol{v}$ therefore appears in the equation corresponding to (2.16). The resulting expression is

$$S(v) = \frac{e_1^2 e^2}{nv\hbar\pi^3}\int d^3k_1 \int d^3k_0 \frac{\boldsymbol{k}\cdot\boldsymbol{v}}{|k^2\varepsilon(\boldsymbol{k},\boldsymbol{k}\cdot\boldsymbol{v})|^2}\,\delta(\omega_1 - \omega_0 - \boldsymbol{k}\cdot\boldsymbol{v}), \tag{2.18}$$

where $k_0 < k_F < k_1$ defines the integration limits. This expression will be discussed in more detail in the following section.

3. Integrated Cross Sections

It is convenient first to study the cross section integrated over all ejection angles, i.e., the energy distribution of ejected electrons. This will be done in the present

section. In addition, the total cross section will be discussed briefly as well as the connection with the stopping power. The results of this section overlap to some extent with those of the study of Ritchie et al. [7-9]

After introduction of the vector $\boldsymbol{k}$ rather than $\boldsymbol{k}_0$ as the integration variable, (2.16) reads

$$d^3\sigma = \frac{e_1^2 e^2}{nv\pi^3\hbar^2} d^3k_1 \int d^3k \frac{\delta\left(-\frac{\hbar k^2}{2m} + \frac{\hbar \boldsymbol{k}\cdot\boldsymbol{k}_1}{m} - \boldsymbol{k}\cdot\boldsymbol{v}\right)}{|k^2\varepsilon(\boldsymbol{k}, \boldsymbol{k}\cdot\boldsymbol{v})|^2} \tag{3.1}$$

with the boundary

$$\boldsymbol{k}\cdot\boldsymbol{v} \geq \frac{\hbar}{2m}(k_1^2 - k_F^2) \geq 0 \tag{3.1a}$$

corresponding to $k_0 < k_F$. By means of spherical coordinates, and integrating, we obtain

$$d\sigma = \iint_{4\pi} d^3\sigma = \frac{2e_1^2 e^2 m}{nv\pi^2\hbar^3} k_1 dk_1 \int \frac{d^3k}{k|k^2\varepsilon(\boldsymbol{k}, \boldsymbol{k}\cdot\boldsymbol{v})|^2} \tag{3.2}$$

with

$$\frac{\hbar}{2m}(k_1^2 - k_F^2) \leq \boldsymbol{k}\cdot\boldsymbol{v} \leq \frac{\hbar}{2m}(2kk_1 - k^2)\ ; \tag{3.2a}$$

Let us now introduce Lindhard's variables z and u, Eqn. (2.9). Eqn. (3.2) becomes

$$d\sigma = \frac{e_1^2\chi^2}{nmv^2} k_1 dk_1 \iint \frac{z\,dz\,du}{|z^2\varepsilon(z,u)|^2} \tag{3.3}$$

with boundaries on the integrals

$$uz \geq \tfrac{1}{4}(k_1^2/k_F^2 - 1) \tag{3.3a}$$

$$u + z \leq k_1/k_F \tag{3.3b}$$

$$u \leq v/v_F\ . \tag{3.3c}$$

Before analyzing (3.3), we also carry out the integration over k_1 in order to obtain the total cross section. This yields

$$\begin{aligned}\sigma &= \int_{k_1 = \mathrm{Max}(k_F, k_F(u+z))}^{k_F\sqrt{1+4uz}} d\sigma \\ &= \frac{e_1^2\chi^2 k_F^2}{2nmv^2} \iint \frac{z\,dz\,du}{|z^2\varepsilon(z,u)|^2} \{4uz\cdot\theta(1-u-z) + [1-(z-u)^2]\theta(u+z-1)\}\end{aligned} \tag{3.4}$$

with the bounds

$$|z-u| \leq 1 \tag{3.4a}$$

$$0 \leq z \tag{3.4b}$$

$$0 \leq u \leq v/v_F. \tag{3.4c}$$

The integration region is the total accessible range for single-particle excitation; the term in the brackets of (3.4) is readily identified as $\frac{8}{\pi} z f_2(z,u)$ in the range $|z-u| < 1$. Therefore, (3.4) can be rewritten

$$\sigma = -\frac{4e_1^2 k_F^2}{\pi n m v^2} Im \int_0^\infty dz \int_0^{v/v_F} du \left(\frac{1}{\varepsilon(z,u)} - 1\right), \tag{3.5}$$
$$|z-u| \leq 1$$

The stopping cross section S is a similar integral; it can be found by adding a factor

$$\hbar(\omega_1 - \omega_0) = \hbar \boldsymbol{k} \cdot \boldsymbol{v} = 2 m v_F^2 u z$$

in (3.5). Then,

$$(S)_{\text{Single Particle}} = \int \hbar(\omega_1 - \omega_0)\, d\sigma = -\frac{24\pi e_1^2 \hbar v_F}{m v^2} Im \int_0^\infty z dz \int_0^{v/v_F} u du \left(\frac{1}{\varepsilon(z,u)} - 1\right) \tag{3.6}$$
$$|z-u| \leq 1$$

which is identical with Lindhard's expression[1] for the stopping cross section, except that the integration is restricted to single-particle excitations, $|z-u| \leq 1$. This was to be expected from the derivation procedure. The expression (3.6) has been studied extensively in ref. 2. The total cross section, Eqn. (3.5), can be evaluated in the same manner. A detailed study has been published recently.[8] Rather than evaluating that quantity separately, we go back to the differential quantity $d\sigma$, and mention some results concerning σ as a check on $d\sigma$ where appropriate.

Fig. 1a shows the area of integration in Eqn. (3.3) for a number of values of k_1/k_F. It is seen that the integral extends over a segment of the stripe $|u-z| \leq 1$; for $v > v_F$ the size of this segment is independent of v in the range of k_1-values limited by

$$1 \leq \frac{k_1}{k_F} \leq 2\frac{v}{v_F} - 1 \tag{3.7a}$$

and decreases towards zero in the range

$$2\frac{v}{v_F} - 1 \leq \frac{k_1}{k_F} \leq 2\frac{v}{v_F} + 1. \tag{3.7b}$$

For $v/v_F \leq 1$, the integration region depends on v for all values of k_1 (Figure 1b).

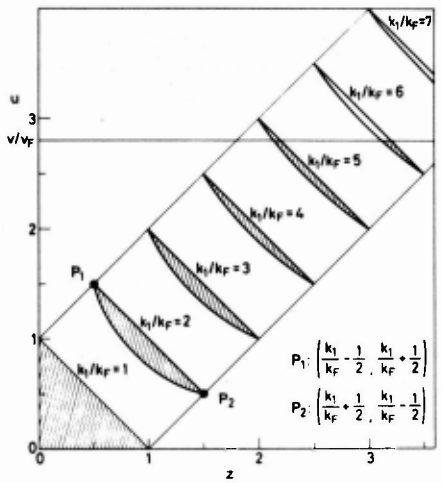

Fig. 1a. Limits of integration for Eqn. 3.3 in the (z,u) plane for $v > v_F$.

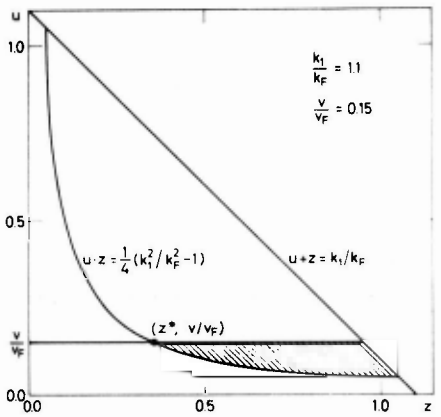

Fig. 1b. Limits of integration in the (z,u) plane for Eqn. 3.3 for $v < v_F$.

These relations provide a classification scheme for the evaluation of $d\sigma$ according to Eqn. (3.3). For practical purposes, it is convenient to include one more dimension in such a scheme, namely the role of the resonance point defined by[2]

$$\varepsilon(z_c, u_c) = 0; \quad u_c = z_c + 1 \tag{3.8}$$

The function $d\sigma$ will normally have a singularity at that value of k_1 where the point P_1 (Fig. 1a) passes through the resonance point (z_c, u_c). According to (3.3c), this is only possible for

$$v \geq u_c v_F \equiv v_c \tag{3.9}$$

Thus, v_c represents a "critical" velocity above which a singularity occurs in the excitation spectrum. From (3.8) and (2.11), we find u_c to obey the relation

$$(u_c - 1)^2 + \frac{\chi^2}{2}\left[1 - u_c \log\frac{u_c}{u_c - 1}\right] = 0. \tag{3.10}$$

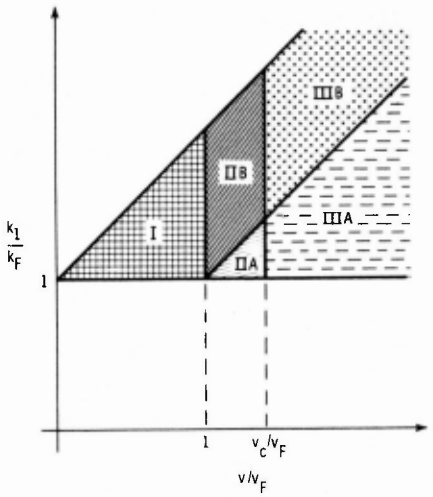

Fig. 2. Portion of (v,k_1) plane showing the classification scheme for projectile velocity and excitation k-vector. Region I, $0< v< v_F$; region II, $v_F< v< v_c$; region III $v_c< v$.
The labels A and B indicate k_1-values for which the reduced integrated excitation spectrum, Eq. (3.22), is independent of v and dependent on v, respectively.

Now, we have three regions of particle velocity (Fig. 2). In region I, $v \leq v_F$, the integral in (3.3) depends on v, and the allowed range of k_1-values is

$$1 \leq k_1/k_F \leq 2\frac{v}{v_F} + 1 \,. \tag{3.11}$$

In region II, $v_F \leq v \leq v_c$, and region III, $v \geq v_c$, the integral (3.3) is independent of v for k_1-values in the range (3.7a), called A, and dependent on v in the range (3.7b), called B; in region III, $d\sigma$ has a singularity at

$$k_c = (2u_c - 1)k_F \,, \tag{3.12}$$

while such a singularity does not occur in region II (nor I).

The singularity in the excitation spectrum due to the resonance in $\varepsilon(z,u)$ at the point (z_c,u_c) results from the excitation of virtual plasmons with wave vector k_c and frequency $\omega_c = v_F k_c u_c$. These plasmons correspond to the shortest wavelength collective excitations which are supportable by the free electron gas.

A. *Analytical Approximation: Region I*

A simple analytic approximation is possible in region I in the limit of $v \ll v_F$. The area of integration in the $z-u$ plane as defined by Eqns. (3.3a-c) is indicated in Fig. 1b, and Eqn. (3.3) reads, to lowest order in v/v_F,

$$d\sigma_{\text{app}} \simeq \frac{e_1^2 \chi^2}{nmvv_F} k_1 dk_1 \int_{z^*}^{1} \frac{z dz}{|z^2 \varepsilon(z,0)|^2} \left(1 - \frac{z^*}{z}\right) \tag{3.13}$$

where

$$z^* = \frac{v_F}{4v} (k_1^2/k_F^2 - 1) , \tag{3.13a}$$

so that

$$d\sigma_{\text{app}} \simeq \frac{e_1^2}{2nmvv_F} k_1 dk_1 \left(\frac{1 - z^*}{\alpha^2 + \chi^2} + \frac{z^*}{\chi \cdot \alpha} \operatorname{arctg} \frac{z^* - 1}{\frac{\chi}{\alpha} + \frac{\alpha z^*}{\chi}} \right) \tag{3.14}$$

with

$$\alpha = \sqrt{1 - \chi^2/3} \tag{3.14a}$$

and

$$0 \leq z^* \leq 1 . \tag{3.14b}$$

In the evaluation of (3.14), the approximation $f_1(o,z) \simeq 1 - \frac{1}{3} z^2$ has been made. * The form (3.14) offers itself for introduction of the excitation energy above the Fermi energy

$$\varepsilon_1 = \frac{\hbar^2}{2m} (k_1^2 - k_F^2) . \tag{3.15}$$

Then

$$z^* = \frac{\varepsilon_1}{2mvv_F} \tag{3.16}$$

and

$$0 \leq \varepsilon_1 \leq 2mvv_F . \tag{3.17}$$

Integration over $d\varepsilon_1$ leads to

$$\int_{z^*=0}^{1} d\sigma_{\text{app}} = \sigma_{\text{app}} \simeq \frac{me_1^2}{2n\hbar^2\alpha^2} \left\{ \frac{\chi}{\alpha} \operatorname{arctg} \frac{\alpha}{\chi} - \frac{\chi^2}{\alpha^2 + \chi^2} \right\} , \tag{3.18}$$

an expression that can be obtained directly by evaluation of (3.4) in the limit

* This approximation is identical with the one used by Lindhard and Winther,[2] but differs from that used by Ritchie.[9]

$v/v_F \ll 1$. Eqn. (3.18) is equivalent with Ritchie's corresponding result (Ref. 9, Eqn. 6.15) when proper account is taken of the fact that his approximation for $f_1(u,z)$ leads to an $\alpha'^2 = 1-\chi^2/2$ in place of α^2 as given by our Eqn. (3.14a).[12]

Going back to the energy spectrum we write (3.14) in the form

$$d\sigma_{\text{app}} = \frac{e_1^2}{2n\hbar^2 v_F v} \frac{1}{(1+2\chi^2/3)} \cdot g\left(\frac{\varepsilon_1}{2mv_F v}\right) \tag{3.19}$$

where

$$g(z^*) = 1 - z^* + z^*\left(\frac{\alpha}{\chi} + \frac{\chi}{\alpha}\right) \operatorname{arctg} \frac{z^* - 1}{\frac{\chi}{\alpha} + \frac{\alpha z^*}{\chi}} \tag{3.20}$$

Fig. 3. Normalized low velocity excitation cross section, Eqns. (3.19) and (3.20).

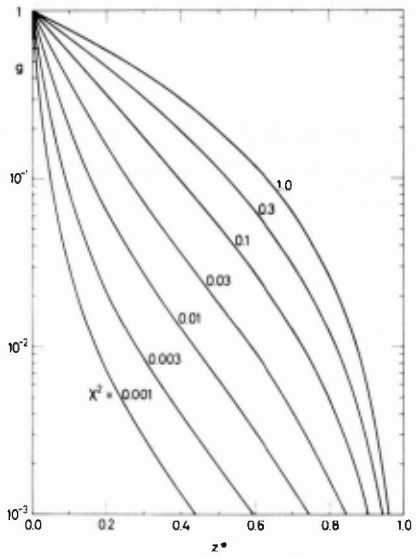

has been plotted in Fig. 3. Note the very simple scaling properties as a function of the primary velocity $v(z^* \propto v^{-1})$. In particular, note that for a wide range of electron densities $(0.03 \leq \chi^2 \leq 0.3)$ the curves for g are almost linear on the semilogarithmic plot of Fig. 3. Figs. 4.a-c shows the ratio of the actual (numerically evaluated) cross section (3.3) and the analytical approximation formula (3.14′) for three different values of the density parameter χ^2, and three values of the ratio v/v_F. We conclude that for rough estimates, the analytical approximation will be satisfactory at all allowed values of the electron energy at values of v not too close to the Fermi velocity.

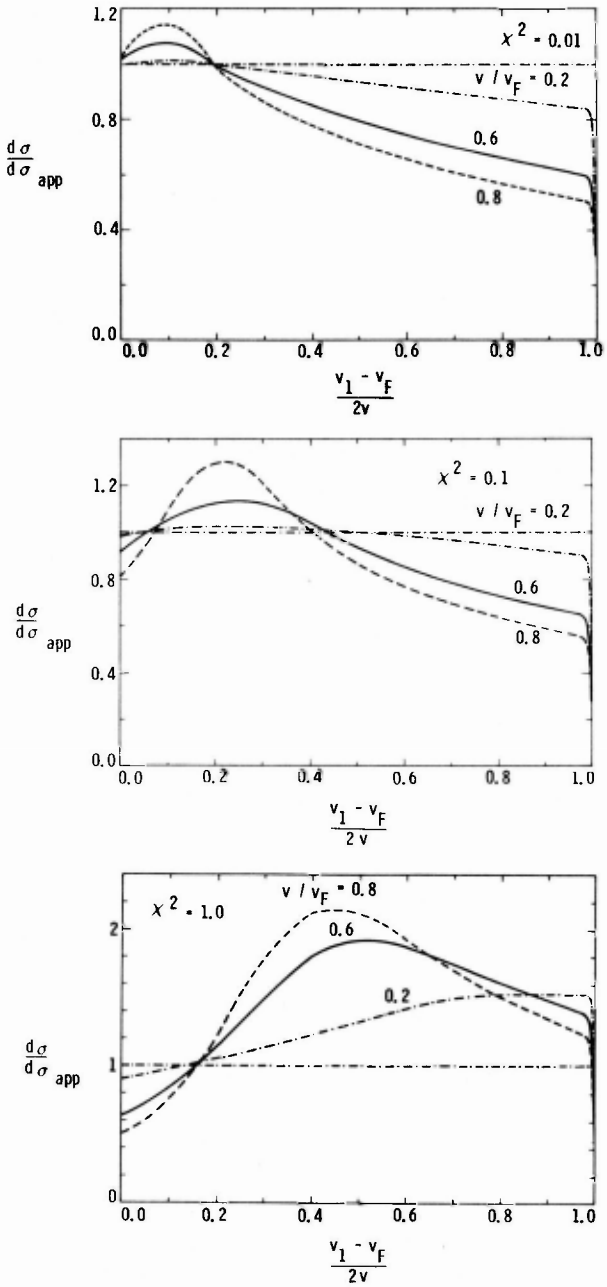

Fig 4. Excitation cross section normalized to the analytical approximation for low incident projectile velocities,
a) $\chi^2 = 0.01$,
b) $\chi^2 = 0.1$,
c) $\chi^2 = 1.0$.

B. *Analytical and Numerical Results: Region II & III*

For $v > v_F$, it is convenient to compare our results with the Rutherford cross section averaged over the Fermi distribution of initial electron velocities. This averaged cross section $d\sigma_R$ is found be setting $\varepsilon \equiv 1$. Eqn. (3.3) yields, then

$$d\sigma_R = \frac{2\pi e_1^2 e^2}{mv^2} \frac{d\varepsilon_1}{\varepsilon_1^2} g_1(\varepsilon_1) \tag{3.21}$$

with

$$g_1(\varepsilon_1) = \begin{cases} 1 & \ldots 0 \le \varepsilon_1 \le 2mv^2 - 2vp_F \\ \left(\frac{v}{v_F}\right)^3 + \frac{3}{16}\left(\frac{\varepsilon_1}{\varepsilon_F}\right)^2 \frac{p_F}{mv - p_1} + & \\ + \frac{1}{4}\left(\frac{\varepsilon_1}{\varepsilon_F}\right)^2 \frac{p_F(p_1 + 2p_F)}{(p_1 + p_F)^2} & \ldots 2mv^2 - 2vp_F \le \varepsilon_1 \le 2mv^2 + 2vp_F \\ 0 & \ldots \varepsilon_1 \ge 2mv^2 + 2vp_F \,. \end{cases} \tag{3.21a}$$

ε_1 is defined in (3.15), and

$$p_1 = \hbar k_1 \tag{3.21b}$$
$$p_F = \hbar h_F \,.$$

In the region where $g_1(\varepsilon_1) = 1$, (3.21) is identical with the conventional Rutherford spectrum for target electrons initially at rest except that the electron energy here is measured from ε_F. The smearing of the edge ($g \neq 1$) is then caused by the ground-state motion in the Fermi gas. The function $g_1(\varepsilon_1)$ has been plotted in Fig. 5 with the expression

$$x = \frac{\varepsilon_1 - (2mv^2 - 2vp_F)}{4vp_F} \tag{3.21c}$$

as the independent variable. It is seen that for $v > 2v_F$, this function is essentially independent of v.

In the more general case, we can write

$$\frac{d\sigma}{d\sigma_R} = \frac{3}{8}\left(\frac{\varepsilon_1}{\varepsilon_F}\right)^2 \iiint \frac{z\,dz\,du}{|z^2 \varepsilon(z,u)|^2} \,, \tag{3.22}$$

where the Rutherford cross section $d\sigma_R$ is the expression (3.21) for $g_1 \equiv 1$. This form does not contain the velocity at all in regions IIA and IIIA, and is therefore a universal function of ε_1, dependent on the density parameter χ^2 only. In

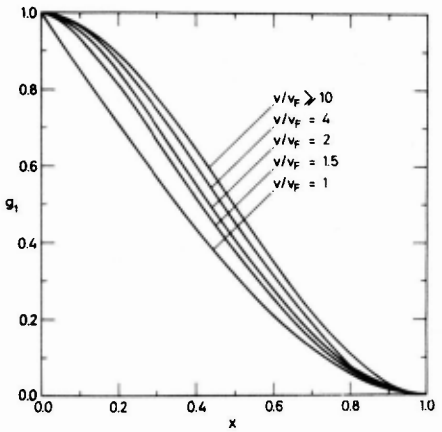

Fig. 5. Cutoff region for $d\sigma_R$, Eqns. (3.21) and (3.21a).

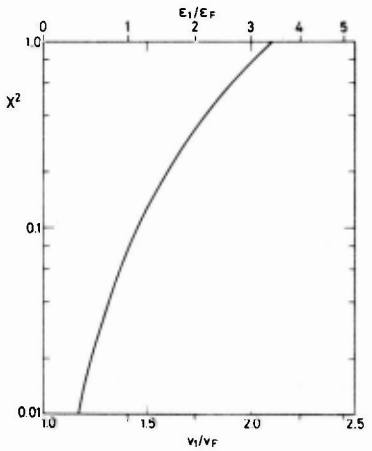

Fig. 7. Peak electron velocity (v_1/v_F) versus electron density, expressed by $\chi^2 = e^2/\pi\hbar v_F$, cf. eqn. (3.25).

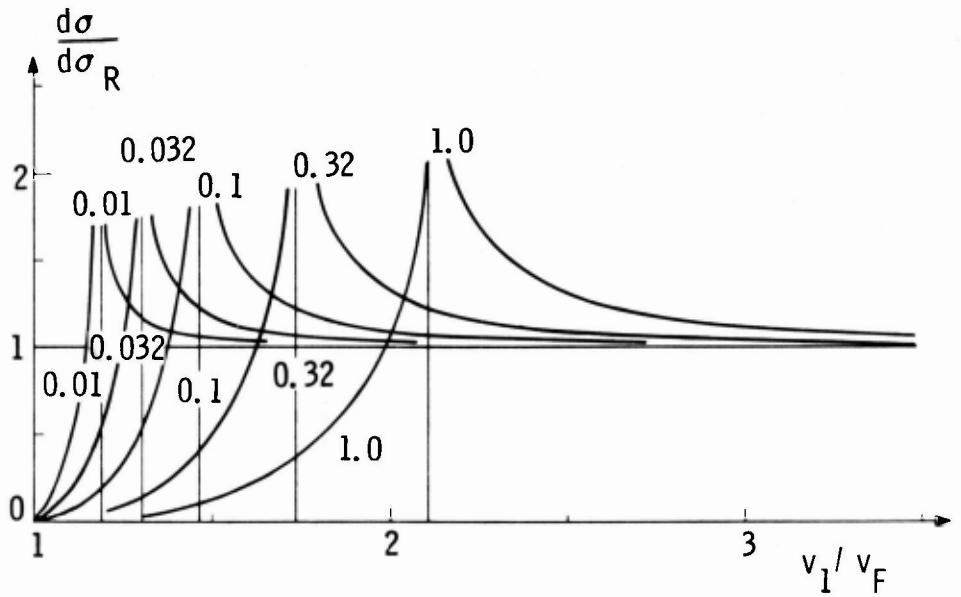

Fig. 6. Excitation cross section $d\sigma$, normalized to $d\sigma_R$, for a series of values of the electron density (cf. eqn. 3.22). For this plot $g_1 = 1$. The numerical integration has been performed by J. Schou.

regions IIB and IIIB, the universal function is to be multiplied by some function $g^1(\varepsilon_1, v; \chi^2)$, with $0 \leq g^1 \leq 1$ and g^1 monotonically decreasing with increasing ε_1. Moreover, for large v (region III) we must have

$$g^1(\varepsilon_1, v; \chi^2) \longrightarrow g_1(\varepsilon_1) \tag{3.23}$$

since $\varepsilon \longrightarrow 1$ at large z, i.e., large values of k.

Fig. 6 shows the expression (3.22), evaluated numerically for $v/v_F \gg 1$. Obviously, $d\sigma$ can be determined directly from Fig. 6 in the regions IIA and IIIA where $g_1 = 1$.

Fig. 6 shows that substantial ($\gtrsim 25\%$) deviations from straight Rutherford scattering occur at electron energies

$$\varepsilon_1 \lesssim 10\varepsilon_F\,, \tag{3.24}$$

the deviations being somewhat dependent on the density parameter χ^2. Most spectacular, of course, is the peak at the position

$$\varepsilon_{1c} = 4u_c(u_c - 1)\varepsilon_F\,, \tag{3.25}$$

following from (3.12), with u_c given by (3.10). This relation has been plotted in Fig. 7. It is seen that the peak position varies slowly with χ^2, and so does the detailed shape of the peak.

Ritchie et al.[7,8] have previously pointed out that the cross section $d\sigma/d\sigma_R$ is a universal function of ε_1, independent of projectile velocity, for $\varepsilon_1 \leq 2mv^2 - 2vp_F$,

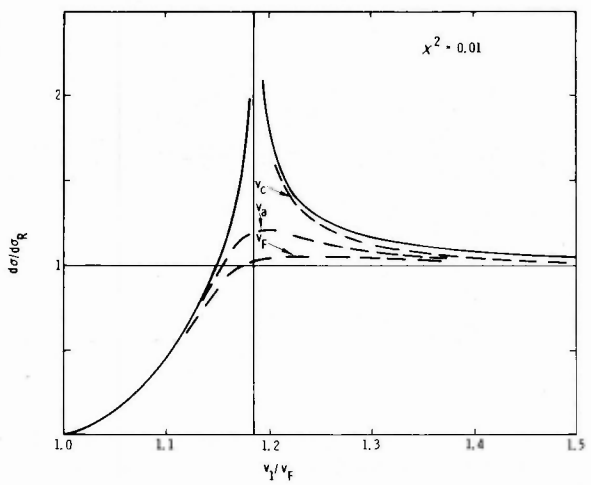

Fig. 8. Excitation cross sections, $d\sigma/d\sigma_R$, in region II. a) $\chi^2 = 0.01$, b) $\chi^2 = 0.1$, c) $\chi^2 = 1.0$.

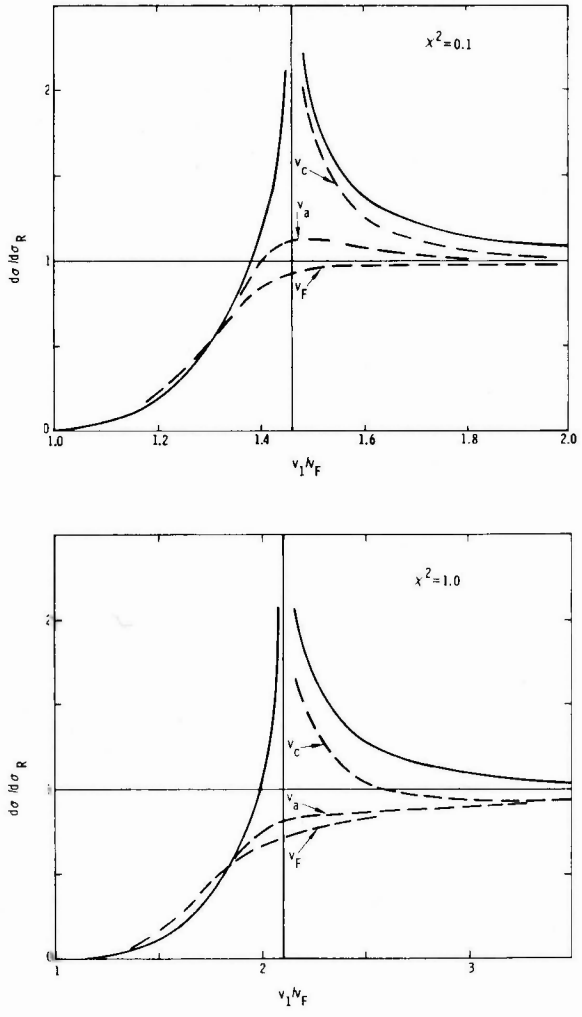

and have evaluated an expression similar to (3.22) for incident electrons. Their spectra also show a peaked behavior with the peak occurring at the position indicated by (3.25).*

Figs. 8a-c show electron spectra, evaluated numerically, and normalized to

*See, for example, Fig. 4 of the second paper of Ref. 7 where the value $r_s = 2.07$ corresponds to $\chi^2 = 0.343$.

Eqn. (3.21), i.e., including that region for which $g_1 < 1$. Curves are shown (dashed) for $v = v_F$, v_a, and v_c, where $v_a = (v_F + v_c)/2$. Also shown are the universal curves from Fig. 6 (solid). (Note the different horizontal scales on the various parts of Fig. 8). The velocity v_F is the boundary velocity between regions I and II, v_c is the boundary velocity between regions II and III, and v_a lies in the center of region II. For the more dense gases ($\chi^2 \leq 0.1$) the presence of a resonance is already noticed at $v = v_a$, although the singularity in the spectrum occurs only for $v \geq v_c$. Also, for these cases it is seen that with v in region III the actual cross section will differ by less than 10% from that determined from the universal curves (providing that the function g_1 is included in $d\sigma_R$). For $\chi^2 > 0.1$ at $v = v_c$, deviations $\sim 25\%$ are seen between $d\sigma/d\sigma_R$ and the universal curve; therefore v must be somewhat greater than v_c before the universal curve becomes an accurate representation of $d\sigma/d\sigma_R$. It should be noted, however, that these deviations are important only for region IIIB in which $d\sigma$ is a rapidly decreasing function of v_1.

4. Doubly Differential Cross Section

In this section, the full angular and energy distribution of excited electrons is analyzed on the basis of eqs. (3.1) and (3.1a). The procedure is very similar to the one sketched in Section 3. We first introduce spherical coordinates for both $\boldsymbol{k}$ and $\boldsymbol{k}_1$, with polar angles θ and θ_1 against $\boldsymbol{v}$ as the axis. Then, eqn. (3.1) reads

$$d^2\sigma = \frac{\chi^2 e_1^2 k_1\, dk_1\, d\eta_1}{2\pi nmv^2} \int \frac{z\,dz\,du\,d\varphi}{|z^2 \boldsymbol{\varepsilon}(z,u)|^2} \cdot \delta\left(\cos\theta\cos\theta_1 + \sin\theta\sin\theta_1\cos\varphi - \frac{k_F}{k_1}(z+u)\right) \tag{4.1}$$

where z, u, and χ^2 have been introduced in Eqns. (2.8) and (2.9), φ is an azimuth, and $\eta_1 = \cos\theta_1$. We also have

$$u = \frac{v}{v_F}\cos\theta\,, \tag{4.2a}$$

and the limit of integration (3.1a) reads

$$4zu \geq \frac{k_1^2}{k_F^2} - 1 \geq 0\,. \tag{4.2b}$$

The integration over φ can be carried out in (4.1), whereafter $d^2\sigma$ reads

$$d^2\sigma = \frac{\chi^2 e_1^2 k_1\, dk_1\, d\eta_1}{\pi nmv^2} \int \frac{z\,dz\,du}{|z^2 \boldsymbol{\varepsilon}(z,u)|^2} \cdot \left\{(1-\eta^2)(1-\eta_1^2) - \left(\eta\eta_1 - \frac{k_F}{k_1}(z+u)\right)^2\right\}^{-1/2} \tag{4.3}$$

with the extra integration condition that the square root be real, i.e.,

$$(1-\eta_1^2)\left[1-\frac{k_F^2}{k_1^2}(z+u)^2\right] \geq \left[\eta-\eta_1\frac{k_F}{k_1}(z+u)\right]^2 \tag{4.4}$$

The condition (4.2a) provides a hyperbolic boundary for the integration in the $z-u$ plane, curve C_1 in Fig. 9, while condition (4.4) provides an elliptical

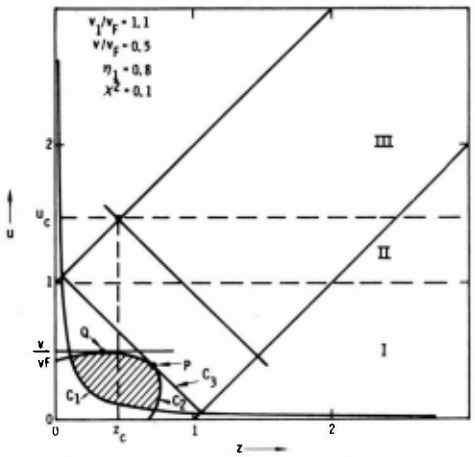

Fig. 9. Limits of integration for Eqn. 4.1 in the (z,u) plane. C_1 corresponds to Eqn. (4.1a), C_2 corresponds to condition (4.4), and C_3 corresponds to condition (3.3b) (Fig. 1).

boundary, curve C_2. We note that the ellipse is tangent to the line $z+u=v_1/v_F$ at point P and also to the line $u=v/v_F$ at point Q, and thus the integration area for $d^2\sigma$ lies *within* the integration area for $d\sigma$ (Fig. 1a), but is tangent to those boundaries. The points P and Q are given by

$$z(P)=\frac{v_1}{v_F}-\eta_1\frac{v}{v_F}, \quad u(P)=\eta_1\frac{v}{v_F} \tag{4.5a}$$

and

$$z(Q)=\frac{v_1}{v_F}\eta_1-\frac{v}{v_F}, \quad u(Q)=v/v_F\,. \tag{4.5b}$$

It is thus clear that the elliptical boundary determines the upper bound on the u-integration.

For fixed v, v_1, Eqns. (4.5a and b) indicate that the points P and Q move along their respective tangent lines as η_1 is varied. This motion is accompanied by rotation and change in magnitude of the axes of the ellipse so that from the standpoint of an observer stationed on either of the tangent lines the ellipse would

appear to roll along the tangent line as η_1 varies. This rolling motion allows the integration area to vary in such a way with η_1 so as to eventually cover the entire boundary region given in Fig. 1a). It is noted that for $\eta_1 = 1$ the points P and Q are identical and the integration area degenerates to a straight line. The cross section $d^2\sigma$ does not become zero in this case, however, because of the integrable singularity in the integrand.

The area of integration in Fig. 9 is only slightly smaller than that for $d\sigma$ (Fig. 1a) so long as P and Q are well separated and P remains within the two straight lines that bound the region of single-particle excitations, $u = z \pm 1$, i.e.,

$$2v\eta_1 - v_F \lesssim v_1 \lesssim 2v\eta_1 + v_F \tag{4.6a}$$

or

$$\frac{v_1 - v_F}{2v} \lesssim \eta_1 \lesssim \frac{v_1 + v_F}{2v}. \tag{4.6b}$$

The integration area decreases rapidly outside this range. An interesting special case, which depends on the form of $\varepsilon(z,u)$, is the position of the resonance. According to (3.12) it occurs at

$$k_c/k_F = 2u_c - 1 \ ;$$

in order to specify the angular region where a peak may be observed, we note that the integration area in Fig. 9 includes the resonance point (z_c, u_c), only when the point P coincides with the resonance point, i.e., according to (4.2)

$$\eta_c = v_F u_c / v \ . \tag{4.7}$$

However, because of the rolling movement of the ellipse one may expect the resonance to be broad as a function of η_1 at a given v_1/v_F in the region near η_c.

We now consider the case where the ellipse becomes tangent to the hyperbola at a single point, i.e., where the two points of intersection degenerate to one. In this case, the integration area has approached zero. This determines the bounds on electron velocity and ejection angle at a given primary velocity. Solving (4.2a) and (4.4) for u^2, and setting the discriminant equal to zero yields

$$\frac{v_1}{2v} - \frac{(2v + v_F)v_F}{2vv_1} < \eta_1 < \frac{v_1}{2v} + \frac{(2v - v_F)v_F}{2vv_1} \ . \tag{4.8}$$

For $v_1 > 2v - v_F$ the right hand side of (4.8) is greater than 1 and the upper bound on η_1 is 1 in this case. This relation is illustrated in Fig. 10. The reader may keep

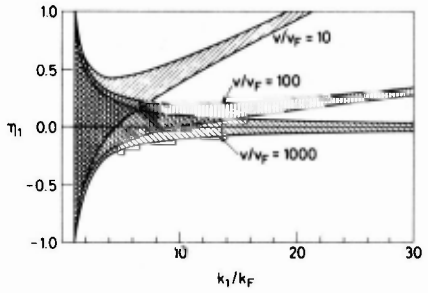

Fig. 10. Values of the excitation velocity, v_1, and cosine of the emission angle, η_1, which are allowed by conservation of energy and momentum.

in mind that it is based only on conservation laws as well as the Fermi distribution at zero temperature, while the dielectric function need not be specified. Thus, no spectral information is contained in Fig. 10 except that the intensity is zero outside the shaded area at any given velocity v.

A. *Analytical Approximation: Region I*

An analytical approximation is possible on Region I in the limit of $v \ll v_F$, as was the case for $d\sigma$. Ignoring u in comparison with z, and working in the (z,η) rather than the (z,u) — plane, we find from (4.3),

$$d^2\sigma = \frac{\chi^2 e_1^2 k_1\, dk_1\, d\eta_1}{\pi n m v v_F} \int \frac{z\,dz}{|z^2\varepsilon(z,0)|^2} \cdot \int \frac{d\eta}{\sqrt{(1-\eta_1^2)(1-z^2)-(\eta-\eta_1)^2}} \tag{4.9}$$

where the area of integration corresponds to the one indicated in Fig. 9, but with the simplifying feature that the ellipse C_2 has its axes parallel to the diagonals on the (z,u) plane. Therefore, (4.9) reads

$$d^2\sigma = \frac{e_1^2\chi^2}{\pi n m v v_F} k_1\, dk_1\, d\eta_1 \left\{ \pi \int_{z_+}^{1} \frac{z\,dz}{|z^2\varepsilon(z,0)|^2} + \int_{z_-}^{z_+} \frac{z\,dz}{|z^2\varepsilon(z,0)|^2} \arccos \frac{r - z\eta_1}{\sqrt{(1-\eta_1^2)(1-z^2)}} \right\} \tag{4.9a}$$

after integration, where

$$r = \frac{v_1 - v_F}{2v}, \tag{4.9b}$$

and z_- and z_+ represent the z coordinates of the upper and lower point of intersection, respectively, of the hyperbola and the ellipse as indicated in Fig. 9.

Again we approximate

$$z^2\varepsilon(z,0) \rightarrow \alpha^2 z^2 + \chi^2$$

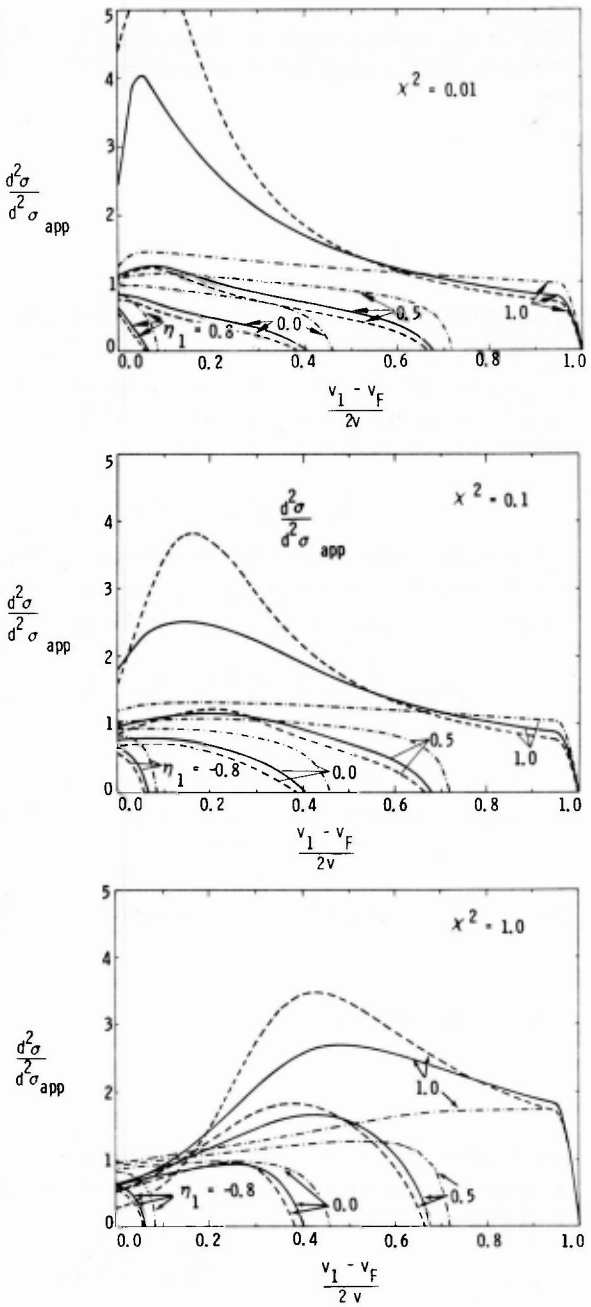

Fig. 11. Low velocity ($v \ll v_F$) values $d^2\sigma/d^2\sigma_{app}$ *vs* $r = (v_1 - v_F)/2v$ for several values of η_1, cf. eqn. (4.10) for $d^2\sigma_{app}$. a) $\chi^2 = 0.01$, b) $\chi^2 = 0.1$, c) $\chi^2 = 1.0$.

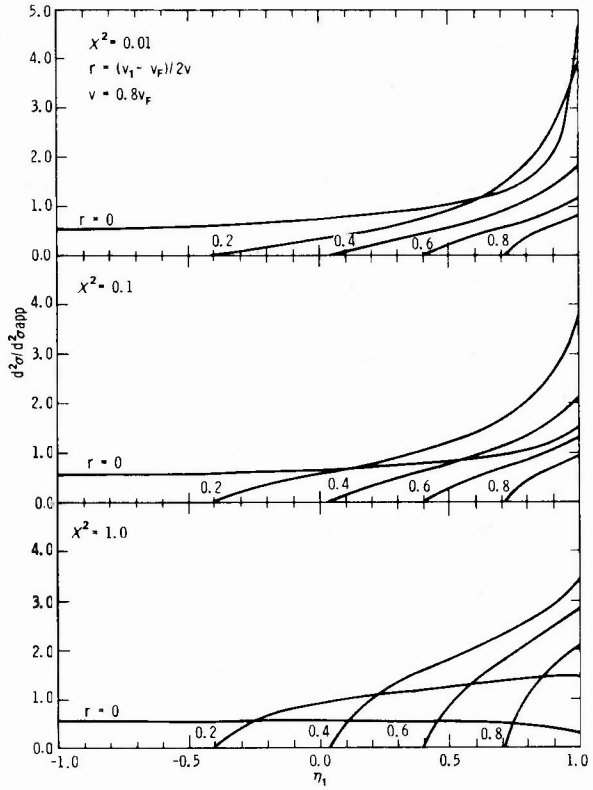

Fig. 12. Low velocity ($v \ll v_F$) values of $d^2\sigma/d^2\sigma_{\text{app}}$ *vs* η_1, for several values of $r = (v_1 - v_F)/(2v)$.

where α is given by (3.14a). Then, the integration in (4.9a) can be carried out. The resultant expression for $d^2\sigma$ is

$$d^2\sigma_{\text{app}} \simeq \frac{3\pi^2}{16} \frac{e_1^2 \hbar}{mv\varepsilon_F^2} \frac{d\varepsilon_1 d\eta_1}{(\alpha^2+\chi^2)} [1 - g_2(r,\eta_1)] \tag{4.10}$$

for $-1+2r \leq \eta_1 \leq 1$; $r \leq 1$,

and where

$$g_2(r,\eta_1) = \frac{(\alpha^2+2\chi^2)r - \chi^2\eta_1}{[(\alpha^2 r + \chi^2\eta_1)^2 + \chi^2(\alpha^2+\chi^2)(1-\eta_1^2)]^{1/2}} . \tag{4.10a}$$

We note also that within this approximation ($v \ll v_F$)

$$\varepsilon_1 = 4\varepsilon_F r v / v_F , \tag{4.10b}$$

i.e., r is proportional to the excitation energy ε_1 above the Fermi level. Figs. 11a-c show spectra, evaluated numerically, normalized to the analytical approximations (4.9) for four different values of η_1, and three values of v/v_F. These curves are analogous to the integrated spectra in Figs. 4a-c, respectively. In Figs. 11, the three values of v/v_F are also 0.2, 0.6, and 0.8, corresponding to the dash-dot, solid, and dashed curves, respectively. The drop to zero on the leading edge of each spectrum occurs because $d^2\sigma_{\text{app}}$ does not go to zero at the right-hand boundaries indicated in Fig. 10, while the exact spectra do.

While the integrated spectra of Figs. 4 do not show large deviations from $d\sigma_{\text{app}}$, the doubly differential spectra of Figs. 11 show considerable departure from $d^2\sigma_{\text{app}}$ for both the forward and backward directions. Despite this, the approximate cross section, Eqn. (4.8), can be quite useful in obtaining spectra for other values of χ^2 by interpolation between curves such as those displayed in Figs. 11. For example, although the numerical values of the absolute cross section differ by more than two orders of magnitude for $\chi^2 = 1$ and $\chi^2 = 0.01$, the *relative* cross sections of Figs. 11a-c differ by a factor less than 2 for most values of η_1, r, and v. This is made particularly evident when angular distributions are compared as in Figs. 12a-c. We thus conclude that the approximate cross section, $d^2\sigma_{\text{app}}$, is quite useful in normalizing the spectra in region I, and that it may be acceptable for many purposes even for velocities v approaching the Fermi velocity.

B. *Analytical and Numerical Results: Regions II and III*

As in the case of the integrated cross section it proves convenient to compare the numerical results for $d^2\sigma$ with the Rutherford cross section, appropriately averaged over the Fermi sphere of initial electron velocities. This cross section $d^2\sigma_R$ is obtained from (4.1) when $\varepsilon = 1$. The resultant expression for $d^2\sigma_R$ is somewhat complicated, but it can be compactly written in terms of several characteristic energies associated with the excitation event. These are

$$\varepsilon_e = \tfrac{1}{2}mv_1^2 = \varepsilon_1 + \varepsilon_F\,, \tag{4.11a}$$

$$\varepsilon_p = \tfrac{1}{2}mv^2 \tag{4.11b}$$

$$\varepsilon_r = \varepsilon_p + \varepsilon_e - 2\eta_1(\varepsilon_e\varepsilon_p)^{1/2} = \frac{m}{2}(\boldsymbol{v} - \boldsymbol{v}_1)^2 \tag{4.11c}$$

and

$$\varepsilon_0 = \varepsilon_p + \varepsilon_r - 2(\varepsilon_p\varepsilon_r)^{1/2} = \frac{m}{2}(v - |\boldsymbol{v} - \boldsymbol{v}_1|)^2. \tag{4.11d}$$

Here, ε_e is the kinetic energy of an excited electron and ε_p the energy of an electron at the projectile velocity, ε_r is the excited electron energy in a system moving with the projectile velocity, and ε_0 is the minimum energy an electron can have in order to be excited to the velocity v_1. The expression which results for $d^2\sigma_R$ is then

$$d^2\sigma_R = \frac{3\pi e_1^2 e^2 (\varepsilon_e \varepsilon_p)^{1/2} g_3(\varepsilon_e, \varepsilon_p, \varepsilon_0, \eta_1)}{4(\varepsilon_F \varepsilon_r)^{3/2}} d\varepsilon_e d\eta_1 \tag{4.12}$$

where

$$g_3 = \varepsilon_e(1-\eta_1^2)[(\varepsilon_e-\varepsilon_F)^{-2} - (\varepsilon_e-\varepsilon_0)^{-2}] - [1-\eta_1(\varepsilon_e/\varepsilon_p)^{1/2}][(\varepsilon_e-\varepsilon_F)^{-1} - (\varepsilon_e-\varepsilon_0)^{-1}]. \tag{4.13}$$

It can be shown that in the limit as $\varepsilon_F \longrightarrow 0$

$$d^2\sigma_R \longrightarrow d\sigma_R \cdot \delta(\eta_1 - v_1/2v)\,, \tag{4.14}$$

where $d\sigma_R$ is the expression given in (3.21) with $g_1 = 1$, and where proper account is taken in the limiting process of the fact that the cross hatched areas in Fig. 10 limit to straight lines as $\varepsilon_F \longrightarrow 0$. The cross section (4.12) can also be obtained by appropriately averaging the classical binary-encounter cross section (Ref. 13, eqn. 15) over a Fermi distribution of initial electron velocities.

The results in section 3 suggest that (4.12) should be an accurate description of $d^2\sigma$ for sufficiently large excitation energy, and comparison with numerically evaluated spectra bears this out. Figures 13a-c show such comparisons for $d^2\sigma$ as a function of electron velocity, v_1, at $\eta_1 = \eta_c$ as defined by (4.6). The projectile velocity, v, was selected for these calculations such that the values of η_c are 0.25, 0.5, and 0.75, for plots a) through c), respectively. These spectra correspond to Fig. 6 for the integrated cross section, $d\sigma$.

One notes that the width of the resonance is relatively independent of the location of the critical angle, and thus that the shape of the resonance is essentially independent of the projectile velocity, as long as v is greater than the critical velocity, v_c (Eqn. (3.9)). This property is further illuminated by the angular distributions one obtains at the critical excitation energy, ε_{1c}, Eqn. (3.25), as shown in Figs. 14a-c, respectively. There it is seen that the angular width of the singularity is almost independent of the projectile velocity. Fig. 15 shows the combined energy and angular dependence of the cross section in the (v_1, η_1) plane. It is nonzero in the cross hatched area defined by Fig. 10, above which is plotted $d^2\sigma/d^2\sigma_R$, for $\chi^2 = 0.1$. The singularity is indicated by the arrow at (x_c, η_c).

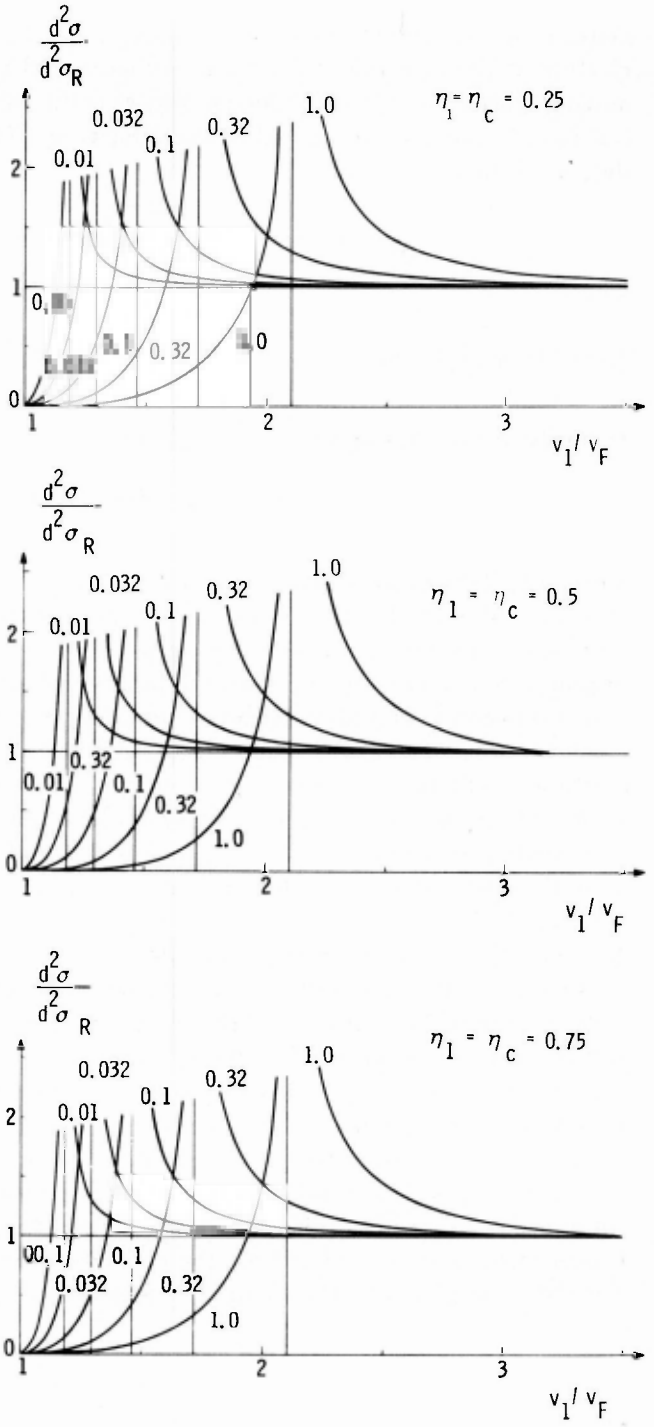

Fig. 13. Normalized double differential excitation cross sections, $d^2\sigma/d^2\sigma_R$, *vs* v_1/v_F for incident projectile velocities such that η_c = a) 0.25, b) 0.5, and c) 0.75.

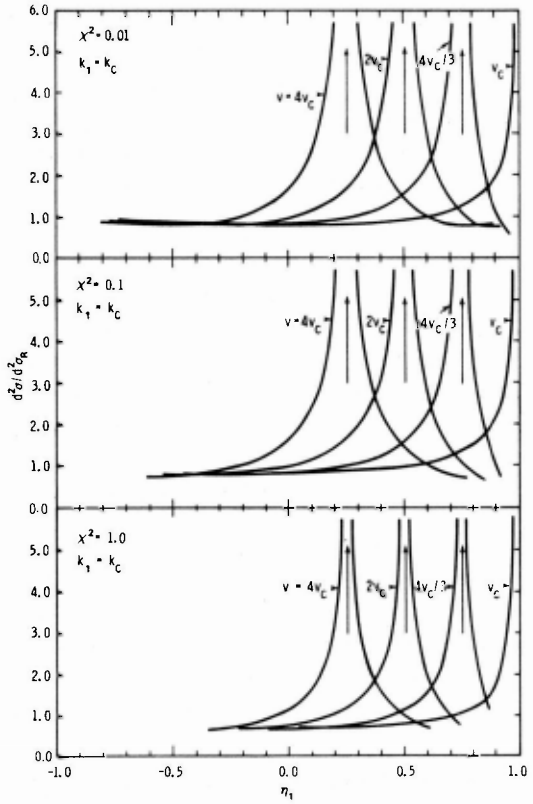

Fig. 14. Normalized double differential excitation cross sections, $vs\eta_1$ at the critical excitation energy. Incident projectile velocities are such that $\eta_c = 0.25$, 0.5, 0.75, and 1.0. a) $\chi^2 = 0.01$, b) $\chi^2 = 0.1$, c) $\chi^2 = 1.0$.

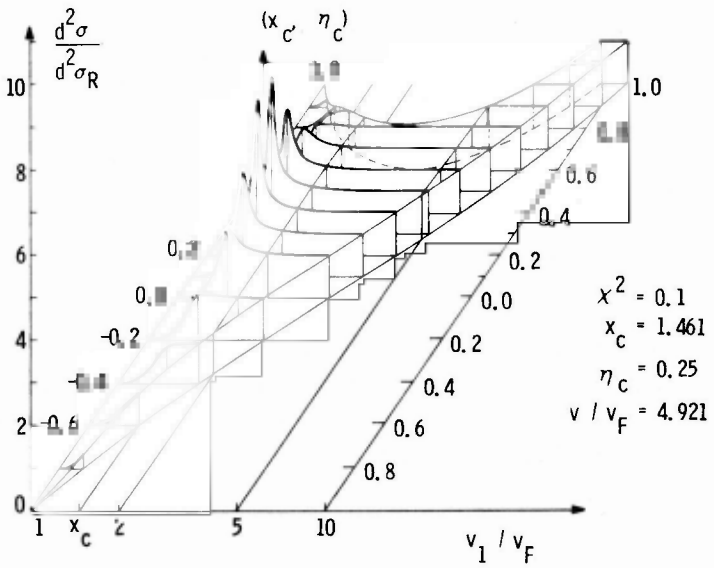

Fig. 15. Three dimensional plot of $d^2\sigma/d^2\sigma_R$ showing both the v_1 and η_1 dependence of the normalized cross section.

From Figs. 13, 14, and 15 it appears that qualitatively we may describe the relative cross section $d^2\sigma/d^2\sigma_R$ as the sum of two parts. One part increases slowly with excitation energy, ε_1, from zero at the Fermi surface to a value approximately equal to 1 for energies greater than ε_{1c}. The other contribution comes from the resonance whose location in the spectrum is determined by Eqns. (3.25) and (4.6), and the shape of which is essentially independent of projectile velocity. This qualitative description also indicates that relatively accurate cross sections can be extracted from Figs. 13 and 14, even for velocities below the critical velocity, by simply translating the angular distributions in η_1 so that the singularity falls at the location determined by (4.6). It should be noted that for $v < v_c$, (4.6) yields values of $\eta_c > 1$, so that the angular distributions are truncated in this case at a value of η_1 which is dependent on v.

5. Summary and Discussion

Single-particle excited-electron spectra have been calculated for heavy atomic projectiles penetrating a free-electron gas. The interactions among the electrons of the gas have been included through the dielectric function of Lindhard. The calculations have been carried out for a broad range of electron densities.

For low incident projectile velocities it proves possible to derive analytical approximations to both single and double differential spectra analogous to Lindhard's low-velocity approximation to the stopping power. The analytical expressions are reasonably accurate for incident velocities not too close to the Fermi velocity of the target electrons. Further, the analytical formulae form a convenient base for the normalization of numerical results, and simplify the process of interpolation between the results presented here.

The low-velocity spectra exhibit characteristic scaling properties expressed by Eqs. (3.19) and (4.10) for the single and double differential cross section, respectively. Apart from normalization, both spectra depend on the excitation energy through the variable

$$r = \varepsilon_1/(2mv_F v)\,, \tag{5.1}$$

and the cross section at $\varepsilon_1 = 0$ is proportional to the reciprocal projectile velocity. These relationships are well corroborated experimentally in low-velocity ion-atom collisions.[14] A more quantitative check on the details of the predicted spectra hinges on a proper averaging procedure over the electron density distribution of the collision partners according to the Thomas-Fermi principle, and is outside the scope of the present paper.

In the limit of very high projectile velocity, the electron spectra follow the laws of classical Coulomb scattering—due account being taken for the initial Fermi distribution of electron velocities—except for excitation energies of the order of the Fermi energy and below, where the behavior is influenced by the mutual interaction between the electrons. A characteristic feature is the occurrence of a resonance at a fixed excitation energy at $\sim$ 1-4 times the Fermi energy, dependent only on the density of the electron gas. Inspection of the double differential electron spectra shows that this resonance occurs at an ejection angle θ_c given by Eq. (4.7),

$$\cos \theta_c = u_c \cdot \frac{v_F}{v}, \tag{5.2}$$

the parameter $u_c (\sim 1.5)$ being determined by Fig. 7 as a function of electron density. It has been shown recently [15] that Eq. (5.2) can be interpreted as a preferential electron ejection in the direction of the Mach angle of the polarization wake[11,16,17] excited by the penetrating particle. The width of the resonance in energy and direction depends on the electron density, and turns out to be roughly proportional with the excitation energy at which the resonance occurs. In atomic systems, the resonance is expected to be broadened due to the finite volume of the atomic electron gas. Resonances of this type do not seem to have been identified experimentally so far.

With regard to predicted spectra for the case of the free Fermi gas, the limiting energies and angles of ejection are given by Fig. 10 as a function of electron velocity, and Figs. 5 and 6 determine the deviations of single differential spectra from straight Coulomb scattering. Similarly, Figs. 13a-c and 14a-c determine the corresponding deviation of the double differential cross section in energy and angular variables, respectively. Numerical tabulations are available.[18] The latter may become useful in particular for intermediate projectile velocities.

Acknowledgements

This work has been supported by a grant of the Danish Natural Science Research Council, which enabled one of us (DKB) to carry out the research reported here. DKB would also like to extend his appreciation to the faculty and staff of Physical Laboratory II of the H. C. Ørsted Institute of the University of Copenhagen for making his stay there an enjoyable and productive experience. Both authors would like to thank lic. scient. Jørgen Schou for assisting in part of the computational work.

References

1. J. Lindhard, Mat. Fys. Medd. Dan. Vid. Selsk. *28*, No. 8 (1954).
2. J. Lindhard and Aa. Winther, Mat. Fys. Medd. Dan. Vid. Selsk. *34*, No. 4 (1964).
3. J. Lindhard, and M. Scharff, Mat. Fys. Medd. Dan. Vid. Selsk. *27*, No. 15 (1953).
4. E. Bonderup, Mat. Fys. Medd. Dan. Vid. Selsk. *35*, No. 17 (1967).
5. See, for example, *Elementary Excitations in Solids* by D. Pines, W. A. Benjamin, New York (1963).
6. Radiation Research, Biomedical, Chemical and Physical Perspectives, O. E. Nygaard et al, editors, Academic Press (1975).
7. V. E. Anderson and R. H. Ritchie, IEEE Transactions of Nuclear Science *18*(6), 141 (1971); R. H. Ritchie, C. J. Tung, V. E. Anderson, and J. C. Ashley, Radiat. Research *64*, 181 (1975); C. J. Tung and R. H. Ritchie, Phys. Rev. B *16*, 4302 (1977).
8. C. J. Tung, R. H. Ritchie, J. C. Ashley, and V. E. Anderson, ORNL-TM-5188 (1976).
9. R. H. Ritchie, Phys. Rev. *114*, 644 (1959).
10. H. Esbensen, Thesis, University of Aarhus (1977).
11. Aa. Bohr, Mat. Fys. Medd. Dan. Vid. Selsk. *24*, No. 19 (1948).
12. Equation 6.15 in reference 9 contains a number of typographical errors (R. H. Ritchie, private communication). When these errors are corrected this equation is identical to our equation 3.18, apart from the different α-value as indicated in the text.
13. E. Gerjuoy, Phys. Rev. *148*, 54 (1966).
14. J. Østgaard Olsen and N. Andersen, private communication.
15. W. Schäfer, H. Stöcker, B. Müller, and W. Greiner, Z. Physik *A288*, 349 (1978).
16. N. Bohr, Mat. Fys. Medd. Dan. Vid. Selsk. *18*, no. 8 (1948).
17. J. Neufeld and R. H. Ritchie, Phys. Rev. *98*, 1632 (1955).
18. D. K. Brice, unpublished.

Indleveret til Selskabet juli 1979.
Færdig fra trykkeriet februar 1980.